Photon rates for heavy-ion collisions from hidden local symmetry

Miklós-Ádám Halász,[1] James V. Steele,[2] Guo-qiang Li,[1] and Gerald E. Brown[1]
[1]*Department of Physics and Astronomy, SUNY at Stony Brook, Stony Brook, New York 11794-3800*
[2]*Department of Physics, The Ohio State University, 174 West 18th Avenue, Columbus, Ohio 43210-1168*
(Received 11 December 1997)

We study photon production from the hidden local symmetry approach that includes π, ρ, and a_1 mesons and compute the corresponding photon emission rates from a hadronic gas in thermal equilibrium. Together with experimental radiative decay widths of the background, these rates are used in a relativistic transport model to calculate single photon spectra in heavy-ion collisions at SPS energies. We then employ this effective theory to test three scenarios for the chiral phase transition in high-temperature nuclear matter including decreasing vector meson masses. Although all calculations respect the upper bound set by the WA80 Collaboration, we find the scenarios could be distinguished with more detailed data. [S0556-2813(98)04307-6]

PACS number(s): 25.75.−q, 12.40.−y, 13.75.Lb, 25.20.Lj

I. INTRODUCTION

Experiments due to be performed over the next few decades are aimed at achieving a quark-gluon plasma, thereby hopefully granting the ultimate confirmation of QCD as the theory of strong interactions and also settling the debate over the phenomenology of hadronic matter at high density. However, data currently available from experiments carried out at the CERN SPS in the form of dilepton and photon spectra offer information relevant to many outstanding issues, such as the enhancement of low-mass dileptons in central heavy-ion collisions reported by the CERES and HELIOS Collaborations [1,2], anomalous J/ψ suppression in central Pb+Pb collisions by the NA50 Collaboration [3], and finally the limit on single photon spectra from central heavy ion collisions set by the WA80 Collaboration [4].

There has been intense theoretical activity in the past few years to predict the behavior of hadronic matter at high density as chiral symmetry restoration and deconfinement are approached. However, the general physical picture of QCD phase transitions is still not agreed upon. Lattice QCD lacks the techniques to surmount the finite-density problem and other models differ in opinion to the important effects. In particular, there is nothing to prohibit chiral symmetry from being restored via the Georgi vector limit [5].

In this limit, the ρ becomes massless. Its longitudinal polarization must disappear, transforming into a scalar-isovector particle identified as the chiral partner of the pion. The a_1 is the chiral partner of the ρ and so also must become massless. The interesting question is the nature of the mass decrease of the vector mesons and whether heavy-ion collisions will be able to distinguish between them. The decrease in general is an effect still in contention although it is able to explain the dilepton spectrum from CERES within a transport code calculation [6,7].

Based on the restoration of scale invariance of QCD for low momentum scales, Brown and Rho [8] suggested that the mass of nonstrange vector mesons should decrease in dense matter, together with the chiral condensate. There are a number of arguments that emerged that are in favor of Brown-Rho scaling [9]. However, finite-temperature calculations based on effective Lagrangians [10,11] and some lattice results [12] find that the ρ mass does not vanish in the chiral limit.

The aim of this paper is to compare the predictions of decreasing in-medium vector meson masses (whether relying on the Georgi vector limit or not) with the WA80 photon spectra. The most important processes are $\pi\pi\rightarrow\rho\gamma$ and $\pi\rho\rightarrow\pi\gamma$ as well as the decay $\rho\rightarrow\pi\pi\gamma$ as determined in Ref. [13]. The a_1 resonance is also important for photon rates, as discussed in Refs. [14–16], and was treated incompletely in the transport calculations of Ref. [17]. Furthermore, different scenarios for the density dependence of matter such as the Georgi vector limit have not been addressed in the context of photon rates in the past. We therefore use the extended hidden local symmetry Lagrangian to make easy tests of different scenarios through the adjustment of the parameters. The Georgi vector limit is possible in the hidden gauge description as described in the next section. The massive Yang-Mills Lagrangian, as used in Ref. [15], is to some extent a special case of this Lagrangian, corresponding to a specific parameter choice and a different gauge-fixing scheme.

In general, the effective parameters—masses and couplings—may be seen as a result of two distinct steps. First, the low-energy limit of QCD defines the physics of hadrons *in free space* due to chiral symmetry breaking and confinement. Second, the physics of hadrons at high density and temperature is obtained through many-body effects with the above mentioned low-energy interaction.

One might argue to what extent this dichotomy is a natural thing. Whether it is suggested by the very existence of hadrons, or is a result of the historic development of strong interaction physics. There is no good reason to exclude medium effects from either of these steps. For instance, finite-temperature lattice QCD calculations, in principle complete, consider ensembles of a very small number of particles. Temperature effects at this level are mainly due to modification of the QCD vacuum, and may be compared to internal structure modifications of hadrons, rather than many-body effects. Traditional many-body calculations, on the other hand, use the same parameters in their basic Lagrangian at all temperatures and densities. Each of these approaches taken separately might miss part of the picture.

In this paper, we do not attempt to predict medium modi-

fications of the vector meson masses. Instead, we assume all medium effects are induced by Brown-Rho scaling of the vector meson masses and the pion decay constant through three different scenarios as presented below. We therefore can work both in free space and at high temperature and density by adjusting the couplings within the hidden gauge theory framework as will be shown in the next section.

The remainder of the paper is structured as follows. In Sec. II we briefly review the hidden local symmetry (HLS) formalism extended to both vector and axial-vector mesons and its fundamental results. Then we propose a scheme of parameter assignment which leaves only the vector meson masses as external parameters. In Sec. III we present our main analytical results, the $\rho\to\pi\pi\gamma$ decay width and cross sections for $\pi\pi\to\rho\gamma$ as well as $\pi\rho\to\pi\gamma$, and show the thermal equilibrium photon rates derived from them. In Sec. IV we discuss different ways to implement Brown-Rho scaling and their effect on the results of the previous section. In Sec. V we describe the transport model we use and then present the predictions for photon rates from S+Au collisions with the different implementations of Brown-Rho scaling. Finally, Sec. VI is devoted to a summary and conclusions.

II. HIDDEN LOCAL SYMMETRY MODEL

We start with a brief review of the extended HLS model. The reader is referred to Ref. [18] for further details. We would like to include the dynamics of both the ρ and a_1 mesons and at the same time have a mechanism which allows for the Georgi vector limit [5]. This has been done for the ρ meson alone using an SU(2) hidden local symmetry [18]. In that case the Lagrangian depends on a single parameter a with the Kawarabayahi-Suzuki-Riazuddin-Fayyazuddin (KSRF) relation [19] $g_\rho=2f_\pi^2 g_{\rho\pi\pi}$ being a general consequence of the theory. Imposing $a=2$ gives the universality of the ρ couplings, a second KSRF relation $m_\rho^2=2g_{\rho\pi\pi}^2 f_\pi^2$, and ρ dominance which are all phenomenologically motivated. The Georgi vector limit is approached as $a\to 1$. In this limit, the ordering of the hidden local symmetry Lagrangian in terms of the number of derivatives can be vindicated since both the π and ρ are light. Away from the vector limit this ordering of terms can still be considered valid.

In order to include the a_1, we need to extend the local symmetry to $\mathrm{SU}(2)_L\times\mathrm{SU}(2)_R$. This increases the number of terms in the most general Lagrangian to give

$$\mathcal{L}=a\mathcal{L}_V+b\mathcal{L}_A+c\mathcal{L}_M+d\mathcal{L}_\pi+\mathcal{L}_{\mathrm{kin}} \tag{1}$$

with the kinetic terms for the vector V_μ and axial-vector A_μ fields included in the last term. In addition we can add a global SU(2)×SU(2) symmetry to describe external vector $\mathcal{V}_\mu$ (including the photon) and axial-vector $\mathcal{A}_\mu$ fields.

Defining the conventional nonlinear σ field for the pion in terms of three SU(2) fields, $U(x)=\xi_L^\dagger(x)\xi_M(x)\xi_R(x)$, we have [18]

$$\mathcal{L}_{V,A}=\frac{f_\pi^2}{4}\,\mathrm{Tr}|D_\mu\xi_L\xi_L^\dagger\pm\xi_M D_\mu\xi_R\xi_R^\dagger\xi_M^\dagger|^2,$$

$$\mathcal{L}_M=\frac{f_\pi^2}{4}\,\mathrm{Tr}|D_\mu\xi_M\xi_M^\dagger|^2,$$

$$\mathcal{L}_\pi=\frac{f_\pi^2}{4}\,\mathrm{Tr}|D_\mu\xi_L\xi_L^\dagger-\xi_M D_\mu\xi_R\xi_R^\dagger\xi_M^\dagger-D_\mu\xi_M\xi_M^\dagger|^2,$$

$$D_\mu\xi_{R,L}=\partial_\mu\xi_{R,L}-ig(V\pm A)_\mu\xi_{R,L}+ie\xi_{R,L}(\mathcal{V}\pm\mathcal{A})_\mu,$$

$$D_\mu\xi_M=\partial_\mu\xi_M-ig(V-A)_\mu\xi_M+ig\xi_M(\mathcal{V}+\mathcal{A})_\mu.$$

The choice $d=1-b+b^2/(b+c)$ ensures the pion kinetic term in $\mathcal{L}$ has a unit coefficient. Fixing the gauge $\xi_M=1$ and $\xi_L^\dagger=\xi_R=\exp(i\pi/f_\pi)$, there is π-a_1 mixing present in $\mathcal{L}_A$ which can be eliminated by the shift

$$A_\mu\to A_\mu+\frac{b}{b+c}\,\frac{1}{f_\pi g}\,\partial_\mu\pi.$$

The gauge choice for A and V could introduce two other unphysical scalar fields (σ and p) that parametrize the decomposition of $U(x)$ above. This also leads to mass generation for these new fields through the usual Stueckleberg construction. However, choosing the unitary gauge rids the Lagrangian of the unphysical fields at merely the expense of making the vector-field propagators nontransverse. Also, the vector part reduces to the Callan-Coleman-Wess-Zumino (CCWZ) effective Lagrangian in this gauge [5]. We will stick to this gauge throughout for convenience.

Unfortunately, upon adding the a_1, the first KSRF relation develops a strong momentum dependence and the decay width $\Gamma_{a_1\to\pi\gamma}$ vanishes. In addition, the width $\Gamma_{a_1\to\rho\pi}$ is half of its experimental value. (For a full discussion of these points see Ref. [18].) These unattractive features can be rectified by including higher derivative terms. The added part is chosen to be [18]

$$\delta\mathcal{L}=-\mathcal{L}_4+\mathcal{L}_5+\mathcal{L}_6,$$

$$\mathcal{L}_4=\frac{i}{4}\,\mathrm{Tr}[\alpha_M^\mu\alpha_M^\nu F_{\mu\nu}^{(L)}+\xi_M^\dagger\alpha_M^\mu\alpha_M^\nu\xi_M F_{\mu\nu}^{(R)}],$$

$$\mathcal{L}_5=-\frac{i}{4}\,\mathrm{Tr}[\alpha_L^\mu\alpha_M^\nu F_{\mu\nu}^{(L)}-\alpha_R^\mu\xi_M^\dagger\alpha_M^\nu\xi_M F_{\mu\nu}^{(R)}]+\mathrm{H.c.},$$

$$\mathcal{L}_6=\frac{i}{4}\,\mathrm{Tr}[\xi_M\alpha_R^\mu\xi_M^\dagger\alpha_M^\nu F_{\mu\nu}^{(L)}-\xi_M^\dagger\alpha_L^\mu\alpha_M^\nu\xi_M F_{\mu\nu}^{(R)}]+\mathrm{H.c.},$$

with $\alpha^\mu=(D^\mu\xi)\xi^\dagger$ and $F_{\mu\nu}^{(R,L)}$ defined as the field strength for the field combination $(V\pm A)_\mu$. For $a=2$ the first KSRF relation $g_\rho=2f_\pi^2 g_{\rho\pi\pi}$ and vector dominance are regained. The a_1 decays take on the reasonable values $\Gamma_{a_1\to\rho\pi}=360$ MeV and $\Gamma_{a_1\to\gamma\pi}=320$ keV.

Saturating the two Weinberg sum rules with the narrow width approximation [20] gives the two relations[1]

$$g_\rho = g_{a_1}, \quad m_{a_1}^2 = \frac{a}{a-1} m_\rho^2 \equiv \frac{m_\rho^2}{r}, \tag{2}$$

which are satisfied for $b=a$ and $c=a/(a-1)$ in Eq. (1). This leaves only the one parameter a to govern the evolution of the Lagrangian towards the Georgi vector limit. For $a=2$, the familiar relation $m_{a_1}^2 = 2m_\rho^2$ is reproduced. This gives $m_{a_1} = 1090$ MeV, whereas the experimental value is $m_{a_1} \simeq 1230$ MeV. This discrepancy suggests that $a=2$ is not the proper value in free space and it should be closer to $a=1.64$.

Setting $a=1.64$ changes the other physical observables as well. First of all, the $\gamma\pi\pi$ vertex is not entirely vector dominated, resulting in a nonzero $g_{\gamma\pi\pi} = 0.18e$ direct coupling to the photon. (The total contribution including the ρ-γ mixing is still, of course, equal to e.) The ρ-coupling universality is modified to become $g_{\rho\pi\pi} = 0.96g$, still within reason. In fact, the two KSRF relations can be written for general a as

$$g_{\rho\pi\pi} = \frac{1}{2} a g (1+\xi_r), \quad m_\rho^2 = \frac{4}{a(1+\xi_r)^2} g_{\rho\pi\pi}^2 f_\pi^2,$$

with $\xi_r = 2r(1-2r)$ and r defined in Eq. (2). Using $f_\pi = 92.4$ MeV and $g_{\rho\pi\pi}^2/4\pi \simeq 3.0$ [21] improves the second KSRF relation prediction for the ρ mass from $m_\rho = 800$ MeV $(a=2)$ to 760 MeV $(a=1.64)$. Notice that Georgi's relation $m_\rho^2 = 4g_{\rho\pi\pi}^2 f_\pi^2$ is reproduced for $a=1$. The pion vector radius for $a=2$, $\langle r^2 \rangle_V^\pi = 0.39$ fm^2, is slightly below the data $\langle r^2 \rangle_V^\pi = 0.44 \pm 0.03$ fm^2. For general a the value is

$$\langle r^2 \rangle_V^\pi = \frac{3(1+\xi_r)}{g^2 f_\pi^2},$$

which for $a=1.64$ results in 0.46 fm^2 in good agreement with the data. The pion polarizability can then be determined from the Das-Mathur-Okubo relation [22] and gives values consistent with data for both values of a.

The decays of the a_1 meson also are modified. The total width is dominated by $\Gamma_{a_1 \to \rho\pi}$ which changes from 360 to 430 MeV with $a=1.64$, still about equal to the experimental value of 400 MeV. The surprise is the radiative decay $\Gamma_{a_1 \to \gamma\pi}$. It changes from 320 to 50 keV as given by the formula

$$\Gamma_{a_1 \to \gamma\pi} = \left(\frac{e}{g}\right)^2 \frac{(3r-1)^2 |\mathbf{p}|^3}{12\pi f_\pi^2}.$$

This is very different from the experimental value 630 keV also obtained by vector meson dominance. This is due to the contribution and interference from the graph with a direct photon. This is responsible for pulling the width down to 320 keV with $a=2$ $(r=1/2)$ and almost vanishing for $a=1.64$ $(r \simeq 1/3)$. Therefore, not assuming total vector dominance in nature actually improves most quantities towards their measured values by about 10% with the exception of the decay width $\Gamma_{a_1 \to \gamma\pi}$ which nearly vanishes to $\mathcal{O}(e^2)$.

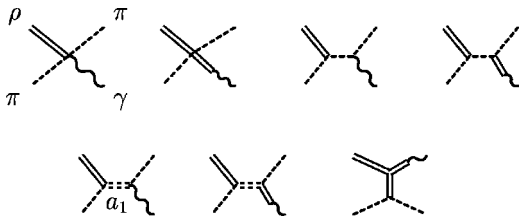

FIG. 1. The general diagrams for the matrix element involving $\rho\pi\pi\gamma$.

III. ANALYTICAL RESULTS

Although we will also consider the effects of the ω, η, and η' mesons, these particles are long enough lived to mostly decay after freeze-out and therefore we can take the experimental values for their partial widths. The only decay abundant enough to consider is then $\rho \to \pi\pi\gamma$. For the photon production from two-body collisions, only $\pi\pi \to \rho\gamma$ and $\pi\rho \to \pi\gamma$ are important enough to consider for the temperature region relevant to heavy-ion collisions at SPS energies [13]. These three processes are all related to the same matrix element quoted in Appendix A. Electromagnetic gauge invariance can easily be checked on our expressions. The contributing graphs are shown in Fig. 1.

First focusing on the decay $\rho \to \pi\pi\gamma$, the result in free space for $a=2$ (1.64) is

$$\Gamma(\rho^0 \to \pi^+\pi^-\gamma) = 1.6 \ (1.8) \ \text{MeV}.$$

Both values are in reasonable agreement with the experimental data 1.5 ± 0.3 MeV [21]. In the same model, we can calculate the radiative decay width of charged rho mesons, and we obtain $\Gamma(\rho \to \pi\pi\gamma) = 0.88$ (0.98) MeV after isospin averaging, showing the $\rho^\pm$ together give slightly less contribution than the ρ^0 alone.

The cross sections for $\pi\pi \to \rho\gamma$ and $\pi\rho \to \pi\gamma$ can be calculated in the same way, and the results are shown in Figs. 2 and 3 for three values of a. A momentum dependent width for the a_1 mesons as calculated in the HLS Lagrangian was included. It is useful to compare our results with those of Kapusta, Lichard, and Seibert [13], which did not include the effects of the a_1 meson.

For $\pi\pi \to \rho\gamma$, the $a=2$ and $a=1.64$ results are similar and near the results of Kapusta *et al.*, within the pertinent values of $\sqrt{s}$. Likewise, the $\pi\rho \to \pi\gamma$ result for $a=2$ (which has a visible bump close to $\sqrt{2}m_\rho$) drops quickly to the Kapusta *et al.*, cross section due to the broadening in the momentum dependent a_1 width. The $a=1.64$ result, however, is larger by almost a factor of 2, showing there is no simple connection between having a small $\Gamma_{a_1 \to \gamma\pi}$ width and the cross section in the $\pi\rho$ channel. Therefore we will use $a=1.64$ for the free space calculations below and not concern ourselves further with the $a=2$ case. As a consistency check,

[1]Adding widths to the resonances changes the quantitative result for the parameter a by less than a percent.

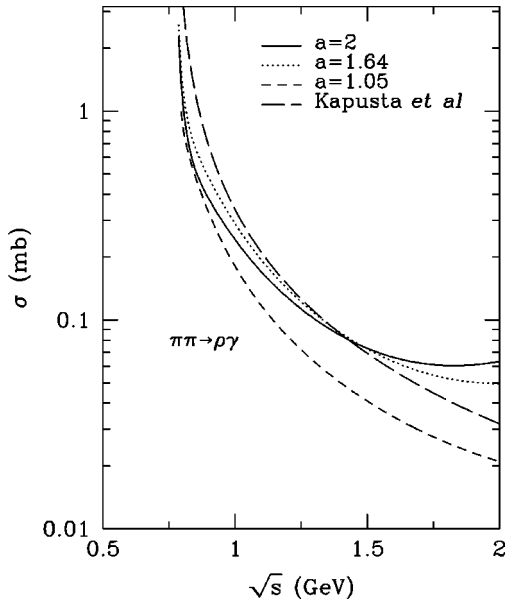

FIG. 2. The total cross section for $\pi\pi\to\rho\gamma$ for $a=2$, 1.64, and 1.05. The value of g is determined by $m_\rho^2=ag^2f_\pi^2$. The result of Ref. [13] is shown for comparison.

our results reduce essentially to those of Kapusta *et al.*, when we turn off the a_1 effects, as they should.

The $a=1.05$ results lead to substantially smaller cross sections, indicating that less photons will be produced from these processes when chiral symmetry restoration is approached. This is especially seen when comparing to the free space result ($a=1.64$). Including the scaling of the parameter g as well will lead to a decrease of the vector meson masses as discussed in the next section. The suppression of cross sections seen here will be counterbalanced by an enhancement from the increase in phase space and the rates will not appreciably change.

Emission rates for photons from a gas of hadrons at thermal equilibrium can be readily computed from the matrix element for a given process. For the process $1+2\to3+\gamma$, the differential rate is given by

$$E_\gamma\frac{dR}{d^3p_\gamma}=\frac{\mathcal{N}}{2(2\pi)^3}\int\frac{d^3p_1}{(2\pi)^3 2E_1}\frac{d^3p_2}{(2\pi)^3 2E_2}\frac{d^3p_3}{(2\pi)^3 2E_3}|\mathcal{M}|^2\times(2\pi)^4\delta^4(p_1+p_2-p_3-p_\gamma)f(E_1)f(E_2)[1+f(E_3)],$$

where $\mathcal{M}$ is the scattering amplitude, $f(x)=[\exp(x/T)-1]^{-1}$ is the Bose-Einstein distribution, and $\mathcal{N}$ is the degeneracy factor which equals the number of distinct incoming states considered in the matrix element. Since the matrix element depends only on the Mandelstam variables $s=(p_1+p_2)^2$ and $t=(p_1-p_\gamma)^2$, we follow Ref. [13] and insert integrals over each of these variables with delta functions ensuring the above definitions. The differential rate can then be expressed in terms of an exact quadruple integral as shown in Appendix B.

For the thermal emission rate from the decay $\rho\to\pi\pi\gamma$, we used the approximate expression given in Ref. [13]. As it is seen from Figs. 4, 5, and 6, our thermal rates for $a=1.64$ are considerably different from those of Song [15] who included the a_1 meson within the massive Yang-Mills approach but did not include a momentum dependent width. For the $\pi\pi\to\rho\gamma$ process, the rates are similar to Song for small photon energy but soon fall below. Although the massive Yang-Mills Lagrangian is a special case of HLS, we have very different parameter choices.

The variable a_1 width is an important effect, leading to a very broad resonance in the s-channel $\pi\rho\to\pi\gamma$ cross section. There the contribution of the a_1 is practically zero for $\sqrt{s}\geqslant1.4$ GeV. However, this does not account for the factor of approximately 3 between our result for the thermal emission rates and those of Song. For the ρ decay, our result is almost identical to Song's, as expected from our agreement on the corresponding decay width. At thermal equilibrium,

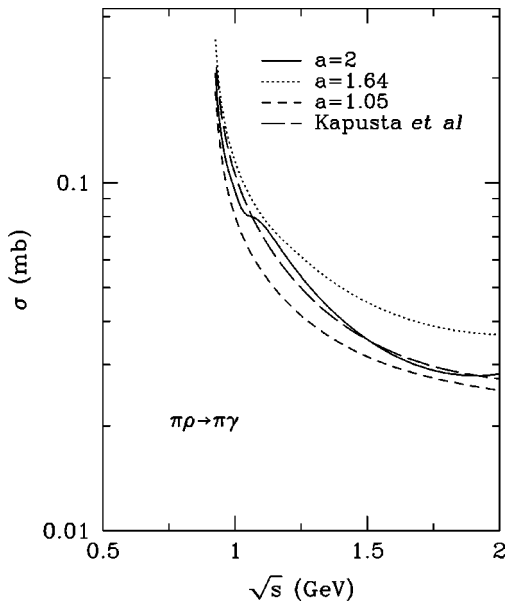

FIG. 3. The total cross section for $\pi\rho\to\pi\gamma$ for $a=2$, 1.64, and 1.05. The value of g is determined by $m_\rho^2=ag^2f_\pi^2$. The result of Ref. [13] is shown for comparison.

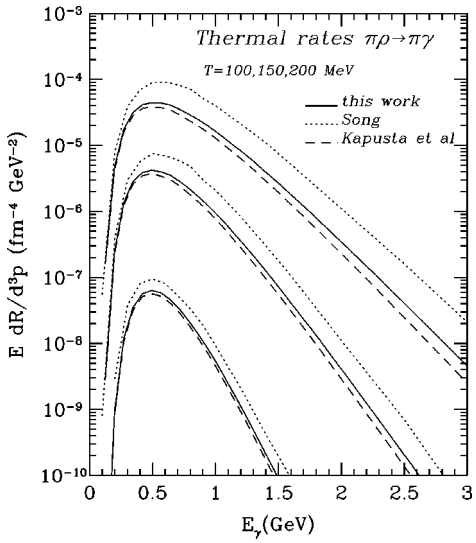

FIG. 4. Thermal rates for the process $\pi\rho\to\pi\gamma$ as compared to those of Song and Kapusta *et al.*

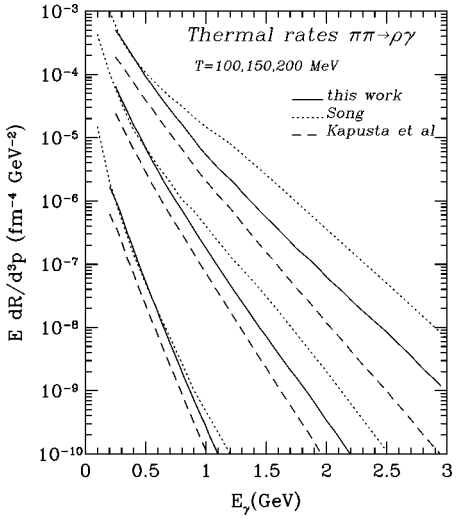

FIG. 5. Same as Fig. 4, for $\pi\pi\rightarrow\rho\gamma$.

the effects from this decay are outshined by those due to the two-body processes by almost two orders of magnitude.

IV. SCENARIOS FOR THE CHIRAL PHASE TRANSITION

The most attractive feature of HLS is that it describes fairly well the dynamics of pions and vector mesons with only three parameters: the pion decay constant f_π, the universal coupling constant g, and the parameter a. From the construction of the HLS Lagrangian, the latter two define the masses of the vector mesons

$$m_\rho^2 = a g^2 f_\pi^2, \quad m_\rho^2/m_{a_1}^2 = (a-1)/a. \tag{3}$$

In practice, this relation may be reversed in order to use the vector meson masses to set the values of a and g.

We set out to use this description for the physics of mesons at high temperature and baryon density. Our basic assumption is that, at least for moderate conditions, the HLS description still holds, only with changed parameter values. In other words, the effects of temperature and medium may be described in terms of changing f_π, m_ρ, and m_{a_1} only.

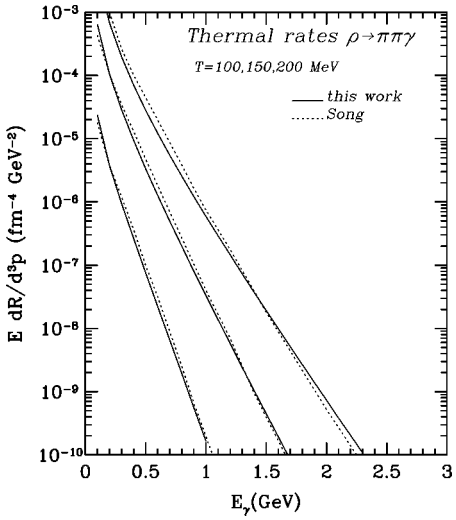

FIG. 6. Same as Fig. 4, for $\rho\rightarrow\pi\pi\gamma$.

Undoubtedly, if our description is valid, renormalization effects as well as temperature and medium effects within the HLS description [10] play a major part in the evolution of our three parameters. On the other hand, there may be more fundamental effects, which can not be predicted from within the effective theory. After all, spontaneous chiral symmetry breaking is a property of full QCD, and the mechanism controlling it may or may not be captured in an approximate description such as ours. Therefore, we do not address within the HLS approach the issue of how the three quantities evolve towards the phase transition. Instead, we will consider a number of scenarios based on very general arguments.

The ρ meson mass has been suggested as a possible order parameter for the chiral phase transition [23]. If the phase transition is of second order, then m_ρ will smoothly decrease towards zero. According to the scaling argument by Brown and Rho [8], all other quantities such as f_π and m_{a_1} will be driven by the ratio m_ρ^*/m_ρ (m_ρ^* is the in-medium ρ mass). Our aim is to find out the effect of such a picture on photon emission from heavy-ion collisions.

Scenario I. The conventional wisdom would be to allow the a_1 mass to drop towards zero along with the ρ mass

$$\frac{m_\rho^*}{m_\rho} = \frac{m_{a_1}^*}{m_{a_1}}.$$

However, this simple scaling will freeze the HLS a parameter at its free-space value as can be seen from Eq. (3). This implies a will never attain its renormalization group fixed point of the HLS theory [18], $a=1$, which would lead to the Georgi vector limit.[2] The dependence of g on the in-medium ρ mass is determined by the scaling dimension of f_π as given by the Gell-Mann-Oakes-Renner relation

$$\frac{m_\rho^*}{m_\rho} = \left(\frac{\langle\bar{\psi}\psi\rangle^*}{\langle\bar{\psi}\psi\rangle}\right)^\alpha ; \left(\frac{f_\pi^*}{f_\pi}\right)^2 = \frac{\langle\bar{\psi}\psi\rangle^*}{\langle\bar{\psi}\psi\rangle} \Rightarrow \frac{f_\pi^*}{f_\pi} = \left(\frac{m_\rho^*}{m_\rho}\right)^{1/2\alpha}.$$

The suggested values for α are 1/3 [8], 1/2 [24], and 1 [25]. Since g scales as $\langle\bar{\psi}\psi\rangle^{\alpha-1/2}$ from the above and Eq. (3), choosing $\alpha=1/3$ would lead to an infinitely strong coupling in the chiral limit contrary to the asymptotic freedom of QCD. The choice of $\alpha=1/2$ is therefore a limiting case, leading to

$$\frac{f_\pi^*}{f_\pi} = \frac{m_\rho^*}{m_\rho}$$

and thus g is frozen to its free-space value just as a is. This prescription is equivalent to the one used in Ref. [17].

[2]A one-loop calculation of the renormalization group equations including the a_1 meson has not yet been done, but even a different fixed point $a=a_0$ will not change the final situations described in this paper.

Scenario II. As opposed to the complete disregard for the renormalization group behavior of a and g, we now take the fixed points to be realized. If a approaches 1 as the ρ mass goes to zero, the ratio m_{a_1}/m_ρ must diverge, as can be seen from Eq. (3). This does not imply the a_1 mass can not vanish, only that it must vanish slower than m_ρ. As a limiting case, however, we take m_{a_1} to be constant[3] and this determines a. Note that now the flow of a and g to their fixed point values of 1 and 0, respectively, are intimately connected such that they conspire to give a constant m_{a_1} as seen in Eq. (3). Of the possible values cited, only $\alpha=1$ for the Brown-Rho scaling drives g to 0. In conclusion, we take

$$\left(\frac{f_\pi^*}{f_\pi}\right)^2=\frac{m_\rho^*}{m_\rho}.$$

This is one way of ''implementing'' the Georgi vector limit, without having to address the issue of the fate of the a_1. If the a_1 becomes massless along with the ρ, then its longitudinal polarization will be a massless scalar, degenerate with the pion.

Scenario III. A different physical picture that may be considered [26] as an alternative to the vanishing of m_ρ in the chiral limit is based on lattice results indicating that m_ρ and m_{a_1} decrease with temperature but become equal at some finite value, not running to zero [12]. If a similar situation occurs with density, we may parametrize it by taking the vector meson masses m_ρ and m_{a_1} as the sum of an invariant degenerate piece $m_{\rm deg}$, which is the same in both, and a piece that scales with the chiral order parameter to some positive power α:

$$\phi\equiv\frac{M^*-m_{\rm deg}}{M-m_{\rm deg}}=\left(\frac{\langle\bar\psi\psi\rangle^*}{\langle\bar\psi\psi\rangle}\right)^\alpha$$

for $M=m_\rho$ and m_{a_1}. It is also possible to consider different values of α for the two vector mesons, but for simplicity we take them equal. Again, f_π will scale with $\phi^{1/2\alpha}$ and so in the limit $\phi\to0$, g is proportional to $\phi^{(\alpha-1)/2\alpha}$, which imposes the choice $\alpha=1$ among the ones mentioned above. Therefore f_π scales with $\phi^{1/2}$ and the matrix elements sharply increase as ϕ approaches 0. In our simulations, where the individual values of the ρ mass are determined by the local mean baryon field, there is a small number of occurrences of $m_\rho^*<0.4m_\rho$. However, these few events alone would generate photons in excess of the WA80 data unless $m_{\rm deg}$ is well enough separated from these lowest values. Our choice of $m_{\rm deg}=0.2m_\rho$ avoids this.

Each of the three scenarios gives distinctly different results as illustrated in Figs. 7 and 8. Figure 7 shows the dependence of the photon production cross sections (for fixed $\sqrt{s}=1200$ MeV) and ρ radiative decay width on the ρ mass.

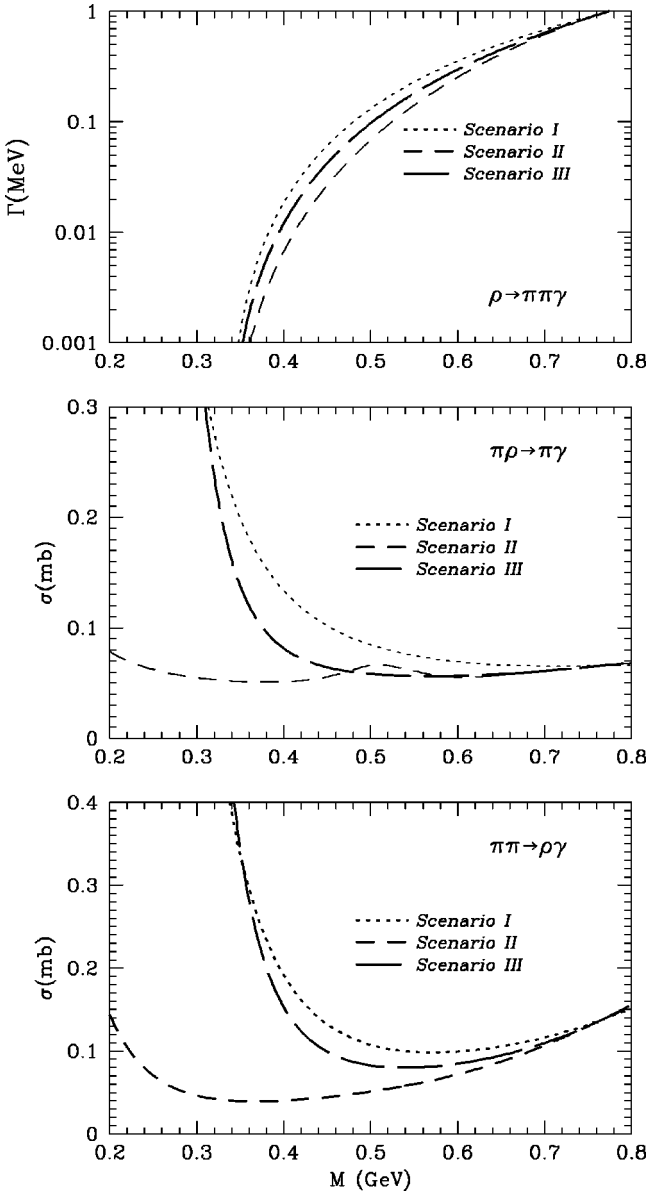

FIG. 7. Photon production cross sections at $\sqrt{s}=1200$ MeV and ρ decay rate as a function of ρ mass, for the three different scenarios.

Since both the strict Brown-Rho scaling of scenario I and the lattice based scaling of scenario III allow both vector meson masses to drop together, we see an increase in the cross sections as the ρ mass decreases. From this point of view, the main difference in the three scenarios is the way in which the a_1 mass decreases: either at the same rate as the ρ, not at all, or faster than the ρ. This leads to a different rate of enhancement for lower ρ masses, and no considerable change for the extreme case of the Georgi-vector limit in scenario II. This can also be seen in Fig. 8 where the ρ mass is fixed at 500 MeV. The a_1 mass reduction in scenarios I and III is accompanied by an increase in the cross sections.

Notice that in Fig. 8 the cross sections for reduced ρ mass tend to increase with $\sqrt{s}$ starting at approximately 1300 MeV. The same behavior is present in the free-space result, only at higher values of s. This is certainly unphysical and comes from the terms with high powers of momenta in the extended HLS Lagrangian introduced by the redefinition of

[3]In our simulations, we expect only relatively small effects from partial chiral symmetry restoration. If the m_{a_1} decreases significantly slower than m_ρ, we may take it constant in the first approximation.

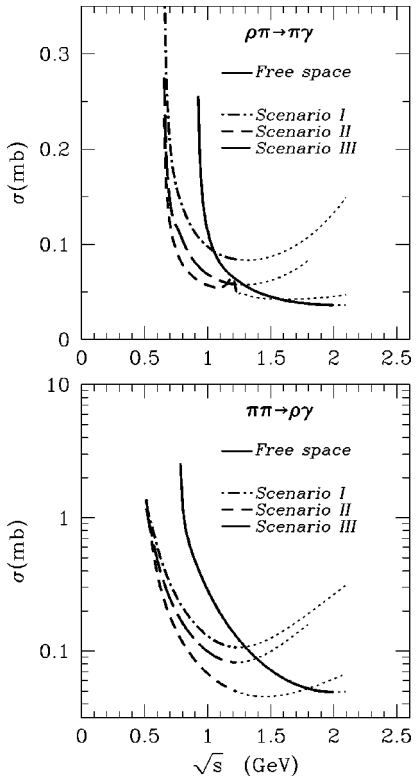

FIG. 8. Photon production cross sections in free space and for a ρ mass decreased to 500 MeV in the three different scenarios. The dotted lines indicate the range where we replace the cross sections by a constant—equal to the value at the start of the dotted line. The value Λ of this cutoff is scaled with m_ρ.

the A_μ field. We are, after all, working with an effective theory which breaks down at high energies. In a more careful analysis, one should interpolate between the effective theory and asymptotically free QCD. For our purposes, we calculate our cross sections up to where they start to increase again ($\sqrt{s}=\Lambda=2$ GeV for the free space case) and then fix the cross section to that final value for larger values of $\sqrt{s}$. The parameter Λ—which can be considered as an effective cutoff parameter to enforce asymptotic freedom, as in most hadronic models—is thus part of our model and is chosen to scale along with m_ρ. In Fig. 8, we show the part of the HLS cross section we use with thicker lines, and the discarded piece with thinner dotted lines above cutoff Λ. Only the high p_t region of our photon spectra are affected by the value of the cutoff. Removing the cutoff altogether, the total photon rates exceed the WA80 limits for $E_\gamma > 1.5$ GeV, but increasing Λ to 3 GeV causes only minor changes in our final results, showing the relatively low sensitivity to having a cutoff.

Naturally, the thermal equilibrium rates shown at the end of Sec. III will increase dramatically for all three scenarios as the vector masses decrease. This is mostly due to the Boltzmann factor. For example, if the ρ-meson mass is reduced to 500 MeV at $T=150$ MeV, the thermal emission rate $\rho\pi \rightarrow \pi\gamma$ increases by about a factor of 6. However, as we will discuss in the next section, this effect is not the only factor to consider when applying these results to heavy-ion collisions. In addition, the total pion multiplicity is constrained by experiment. Whereas the thermal rate calculation corresponds to a grand-canonical ensemble of mesons which can produce excess pions at will, the real situation in heavy-ion collisions is closer to an ensemble with fixed pion number constrained by the hadronic observables.

V. PHOTON SPECTRA IN HEAVY-ION COLLISIONS

In studying medium effects in heavy-ion collisions, relativistic transport calculations [27,28] based on the Walecka-type model have been quite useful, providing a thermodynamically consistent description of the medium effects through the scalar and vector fields. In heavy-ion collisions at CERN-SPS energies, many hadrons are produced in the initial nucleon-nucleon interactions. This is usually modeled by the fragmentation of strings, which are the chromoelectric flux tubes excited from the interacting quarks. One successful model for taking into account this nonequilibrium dynamics is the RQMD model [29]. To extend the relativistic transport model to heavy-ion collisions at these energies, we have used as initial conditions the hadron abundance and distributions obtained from the string fragmentation in RQMD.

Specifically, we obtain from the RQMD model (version 2.1) the chemical composition (hadron abundance), and their spatial and momentum distributions after the string fragmentation. As shown in Refs. [6,7], the initial conditions based on the RQMD string fragmentation and the initial conditions based on thermal and chemical equilibrium assumptions lead to very similar dilepton spectra. We expect that our predictions for photons spectra will not be very sensitive to the particular initial conditions we use.

Further interactions and decays of these ''primary'' hadrons are then taken into account through a conventional relativistic transport model. We include nonstrange baryons with masses below 1.72 GeV, as well as Λ, $\Lambda(1405)$, Σ, and $\Sigma(1385)$. For mesons we include π, η, ρ, ω, η', a_1, and ϕ, as well as K and $K^*(892)$. Baryons are propagated in their mean fields, which are assumed to be the same for all nonstrange baryons. The mean fields for hyperons are assumed to be 2/3 of that for nonstrange baryons, based on the simple quark counting rule. The meson masses are all reduced in accordance with the mean field [6], the only exception being the a_1 mass which is varied according to the three scenarios of Sec. IV.

In addition to propagation in mean fields, hadrons also interact under stochastic two-body collisions. For baryon-baryon interactions, we include both elastic and inelastic scattering for the nucleons $\Delta(1232)$, $N(1440)$, and $N(1535)$. Their cross sections are either taken from Refs. [30, 31] or obtained using the detailed balance procedure [32]. The meson-baryon interactions are modeled by baryon resonance formation and decay. For example, the interaction of a pion with a nucleon proceeds through the formation and decay of any of the N or Δ resonances from the $\Delta(1232)$ up to the $N(1720)$. The formation cross sections are taken to be of the relativistic Breit-Wigner form. The meson-meson interactions are either formulated through resonance formation and decay when the intermediate meson is explicitly included in our model, such as the a_1 meson, or treated as a direct elastic scattering with a cross section estimated from various theoretical models [6].

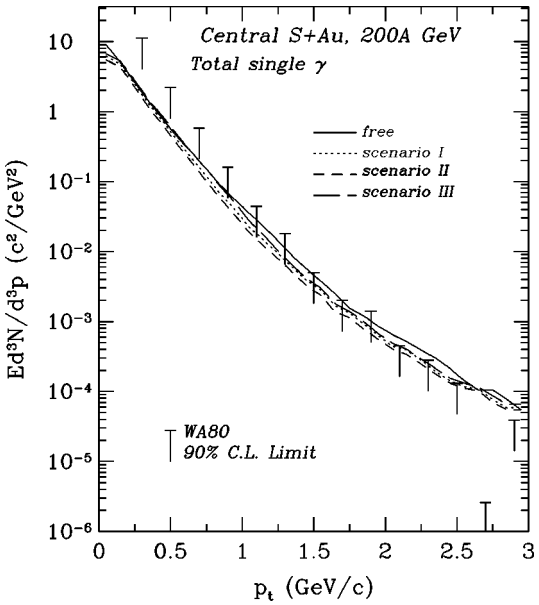

FIG. 9. Total thermal photon spectra in central S+Au collisions at 200*A* GeV for the different scenarios discussed.

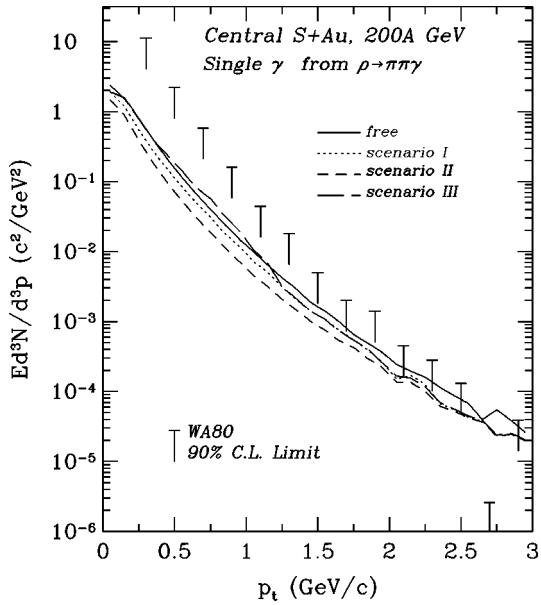

FIG. 10. The same as Fig. 9, for $\rho \rightarrow \pi\pi\gamma$.

Photon creation is taken into account during the evolution of the transport code through decays or two body processes. The experimental data for ω and η' decays are used as these particles are long lived and mostly decay after escaping into free space. Photons can also be produced from the decay of baryon resonances. These contributions are usually neglected in hydrodynamical calculations [33,34], but are included here through experimentally measured radiative decay widths [21]. Baryon contributions are found to be much smaller than those coming from mesons, as pointed out in Ref. [17]. Otherwise, we include the three main contributors to photon production, $\rho \rightarrow \pi\pi\gamma$, $\pi\pi \rightarrow \rho\gamma$, and $\pi\rho \rightarrow \pi\gamma$ as calculated in the previous sections and modify the two fundamental parameters a and g of the HLS Lagrangian according to each of the three scenarios mentioned above.

In Fig. 9 we compare our thermal photon spectra with the upper bound of the WA80 Collaboration. Overall the results are below the upper bound for photons with transverse momenta well below 1 GeV. For higher transverse momenta, our results touch the upper bound of the experimental data. These observations are essentially the same as those of Ref. [17], although the contribution from two-body collisions at high transverse momenta now becomes comparable to that of meson decay, due to a more realistic treatment of a_1 effects. This shows that whether the vector meson masses are reduced or not, the rates do not change much since the opening up of phase space is balanced against a decrease in the coupling constants.

The fact that there is no dramatic increase in photon emission rates would seem to contradict the naive expectations of thermal rate calculations. Regardless of whether the dropping mass scenario is invoked or not, any photon spectrum calculation must at the same time fit the observable pion multiplicity. Through the use of a complete transport calculation as described above, this quantity can be consistently obtained. As shown in Ref. [6], this could be achieved in a thermal model by either decreasing the vector meson mass or increasing the pion chemical potential by hand. Thus, for a meaningful comparison with the dropping mass scenarios, one would need to use a large chemical potential in the bare mass scenario, which would push up the thermal rates. In this paper, however, we do not use thermal equilibrium initial abundances. Instead, we evolve the system from the same initial RQMD output for all cases considered. This procedure guarantees the correct final pion yield without additional assumptions such as a pion chemical potential [7].

With a dropping ρ mass, the ρ number increases in the initial stage mainly through the process $\rho \leftrightarrow \pi\pi$. This, however, is also the dominant decay mode for the ρ and so the pions are eventually regained at freezeout. The three $\rho\pi\pi\gamma$ photon-producing processes discussed in detail above are not enhanced dramatically if the number of ρ mesons increase because this is achieved at the expense of reducing the number of pions. As a result, $\rho\pi \rightarrow \pi\gamma$ is neither favored nor disfavored and the other two processes $\pi\pi \rightarrow \rho\gamma$ and $\rho \rightarrow \pi\pi\gamma$ are balanced against each other. Although all three scenarios are close to the free space result, the largest change comes to scenario II and the Georgi vector limit, which is reduced by almost a factor of 2 in the final rates as seen in Fig. 9.

This variation in the three scenarios can be seen better by breaking the rates up into the important contributions. This is shown in Figs. 10, 11, and 12 for the $\rho \rightarrow \pi\pi\gamma$, $\pi\pi \rightarrow \rho\gamma$, and $\pi\rho \rightarrow \pi\gamma$ rates, respectively. The main contribution can be seen to come from ρ decay, which is larger than what one would expect from the thermal rates of Sec. III. This is a result of the spread of the actual ρ masses around the central value in the transport simulation. The decay rates are driven by phase space, and there is a net gain from the instances of higher mass which is not compensated by losses from lower values. The largest value to the decay rates comes from scenario III in which both masses drop, but a increases as the ratio of the ρ and a_1 mass approaches 1. The lowest rates come from scenario II as one would expect from the cross sections.

It is also interesting to note how similar scenario I is to the free rates in all three figures. This is because Brown-Rho

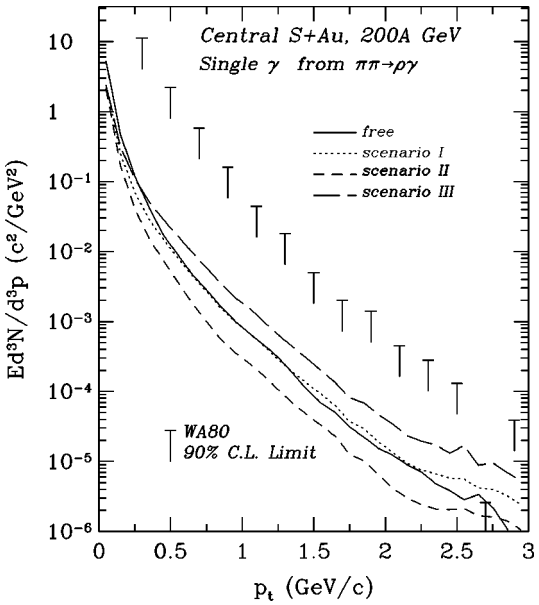

FIG. 11. The same as Fig. 9, for $\pi\pi\rightarrow\rho\gamma$.

scaling for the a_1 meson does not allow either of the two parameters of the HLS Lagrangian to change. The widest range in values among the scenarios comes in the $\pi\pi\rightarrow\rho\gamma$ rates which give a spread of almost an order of magnitude between scenario III (largest) and scenario II (smallest). One can see from Fig. 8 that this process has a larger spread between scenarios in terms cross sections, too.

It is interesting that in total, all three scenarios as well as the free rates touch the upper bounds set by WA80 for large p_t. If other processes such as $a_1\pi\rightarrow\rho\gamma$ were included, they would also feed into this high momentum region and possibly push the rates past the upper bounds. One must be cautious, however, in drawing conclusions in terms of absolute values of the photon rates at high p_t even though we cut off the unphysical high-momentum dependence of our cross sections as discussed at the end of Sec. IV. Needless to say,

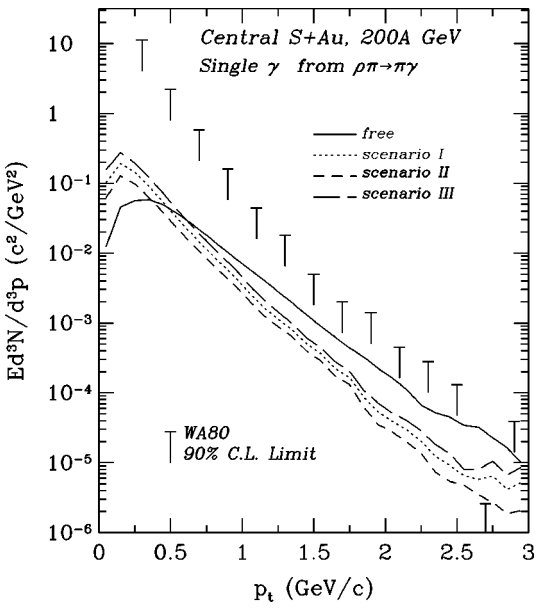

FIG. 12. The same as Fig. 9, for $\pi\rho\rightarrow\pi\gamma$.

results from WA98 and future photon measurements are needed to properly interpret the discrepancy with the present data.

With excellent data in the photon spectra, one could possibly distinguish between the three broad scenarios set forth in this paper. However, given the extremely poor signal to noise ratio for the photons, the experimental uncertainty is too large to say whether one or another of the curves in Fig. 9 is right. One might rank the scenarios in order of decreasing total photon rate. Then, the free-space result and scenario III seem more likely to exceed the upper bounds for the region $p_t<1.75$ GeV than scenarios I and II. Both the free-space result and scenario III are strong in this region for ρ decay. The free-space result outshines all other scenarios for $\rho\pi\rightarrow\pi\gamma$, while scenario III dominates for $\pi\pi\rightarrow\rho\gamma$. Except for ρ decay above 2 GeV, scenario II gives the lowest predictions. Also, it is the only one to have the same slope as the WA80 limits.

VI. SUMMARY AND CONCLUSIONS

The purpose of this study is to investigate the effect of dropping in-medium vector meson masses on photon spectra from heavy-ion collisions. This has been done earlier for dilepton spectra [6] and for photon spectra [17]. In the case of photon spectra, the effect of the a_1 has to be included [14], since it is potentially important.

We recalculated three processes important for photon production in heavy-ion collisions using the extended hidden local symmetry Lagrangian [18] with the proper a_1 mass. We find that the contribution of the a_1 as intermediate state is relatively small, in contrast to results found in earlier models [14,15], but closer to the results in Ref. [16]. It would be interesting to see whether this is indeed a genuine physical effect by looking at alternative formulations of HLS. In particular, the π-a_1 mixing is taken care of now by a shift of the a_1 field whereas using one of the unphysical fields that appear in nonunitary gauges could have the same effect without modifying the $a_1\pi\gamma$ vertex. Both the $a_1\rightarrow\pi\gamma$ decay width and the s- to d-wave ratio in a_1 decay should be used to identify the most advantageous approach.

However, the small effect of the a_1 meson lies in something even more basic: the linear relation in the HLS between the coupling g and the vector meson masses. Therefore, as temperature and density increase, the masses drop in agreement with Brown-Rho scaling [8] and the couplings are driven to zero in accordance with asymptotic scaling. This suppresses the rates when density corrections are taken into account.

Nevertheless, using only the vector and axial-vector meson masses as input parameters our model reasonably predicts the vector and axial-vector meson decay widths. Our predictions for thermal photon emission rates from a hadronic gas through the processes $\rho\pi\rightarrow\pi\gamma$, $\pi\pi\rightarrow\rho\gamma$, and $\rho\rightarrow\pi\pi\gamma$ are within the range of similar results in the literature. The rates for $\rho\pi\rightarrow\pi\gamma$ are slightly higher than those of Kapusta *et al.* [13], but a factor 2–3 lower than those of Song [15].

We considered three different scenarios for the in-medium evolution of m_ρ and m_{a_1} in an attempt to understand the differences in signals they would give: strict Brown-Rho

scaling where the ratio m_ρ/m_{a_1} stays fixed, an extreme case of the Georgi-vector limit where m_{a_1} is fixed, and a schematic model inspired by finite temperature lattice results. We simulated single photon spectra in central S+Au collisions at SPS energies using the relativistic transport model that has been used to study dilepton spectra in the same reactions. We included photons from the background sources of π^0 and η decays, as well as thermal sources such as meson decays, decays of baryon resonances, and two-body processes. We found that more than 95% of single photons come from the decays of π^0 and η. The thermal photons account for only less than 5% of all single photons, in agreement with the experimental observation made by the WA80 Collaboration. We compared our thermal photon spectra with the experimental upper bound extracted by the WA80 Collaboration. Overall, the results were all comparable to each other for the total rate, none of them exceeding significantly the experimental bounds. For $p_t<2$ GeV, the largest photon yields were found for the lattice-inspired scenario and the simulation without dropping masses. The Georgi-vector limit case gives the lowest yield in this range. It slightly exceeds the upper bounds of WA80 for large p_t, but a fully consistent high energy behavior is a matter of further study.

In conclusion, we find that in the extended hidden local symmetry approach the role of the a_1 for the processes we considered is less important than it is generally thought. We showed that one can implement the dropping in-medium ρ mass and Brown-Rho scaling without violating the existing experimental limits for photon production. Furthermore, there are indications that different scenarios lead to experimentally distinguishable predictions.

ACKNOWLEDGMENTS

We thank Charles Gale, Mannque Rho, and Jac Verbaarschot for stimulating discussions and a critical reading of the manuscript and Madappa Prakash, Ralf Rapp, Edward Shuryak, and Heinz Sorge for useful discussions. This work was supported in part by the US DOE Grant No. DE-FG02-88ER40388 and by the National Science Foundation under Grant Nos. PHY-9511923 and PHY-9258270.

APPENDIX A: MATRIX ELEMENTS

For $\rho^a(p)\to\pi^b(p_1)\pi^c(p_2)\gamma(k)$, the matrix element $\mathcal{M}$ shown diagrammatically in Fig. 1 is given by the addition of the following four expressions ($r=m_\rho^2/m_{a_1}^2$):

$$\mathcal{M}_1=\epsilon^{ace}\epsilon^{3be}\frac{e}{2gf_\pi^2}\{m_\rho^2\epsilon_1\cdot\epsilon_2+2r(\epsilon_1\cdot\epsilon_2 p_2\cdot p-\epsilon_1\cdot p_2\epsilon_2\cdot p)+2r^2(\epsilon_1\cdot\epsilon_2 p_1\cdot p_2-\epsilon_1\cdot p_1\epsilon_2\cdot p_2)\}+(p_1,b)\leftrightarrow(p_2,c),$$

$$\mathcal{M}_2=\epsilon^{a3e}\epsilon^{bce}\frac{e}{gf_\pi^2}\left\{(\epsilon_1\cdot p_1\epsilon_2\cdot p+\epsilon_1\cdot k\epsilon_2\cdot p_1-\epsilon_1\cdot\epsilon_2 p_1\cdot k)\,\frac{\xi_r(p_1+p_2)^2+m_\rho^2}{(p_1+p_2)^2-m_\rho^2}-\xi_r\epsilon_1\cdot p_1\epsilon_2\cdot p_2\right\}+(p_1,b)\leftrightarrow(p_2,c)$$

$$\mathcal{M}_3=2age(1+\xi_r)\epsilon^{ace}\epsilon^{3be}\frac{\epsilon_1\cdot p_2\epsilon_2\cdot p_1}{(p_1+k)^2-m_\pi^2}+(p_1,b)\leftrightarrow(p_2,c),$$

$$\mathcal{M}_4=\frac{e}{gf_\pi^2}\epsilon^{ace}\epsilon^{3be}\left\{rW\cdot\epsilon_2+(3r-1)\frac{(p_1\cdot k\epsilon_2\cdot W-\epsilon_2\cdot p_1 k\cdot W)}{(p_1+k)^2-m_{a_1}^2}\right\}+(p_1,b)\leftrightarrow(p_2,c),$$

with $\xi_r=2r(1-2r)$ and

$$W^\mu=\epsilon_1\cdot p_2[(4r-1)p^\mu-rp_2^\mu]-[(4r-1)p_2\cdot p+rp_2\cdot(p_1+k)]\epsilon_1^\mu.$$

As required by gauge invariance, the total matrix element $\mathcal{M}$ vanishes under the replacement $\epsilon_2\to k$.

APPENDIX B: DIFFERENTIAL THERMAL RATE

For the process $1+2\to3+\gamma$ we define $s=(p_1+p_2)^2$, $t=(p_1-p_\gamma)^2$. With $E_3=E_1+E_2-E_\gamma$, introduce

$$q_1=m_1^2-t,\quad q_2=s+t-m_1^2-m_3^2,$$

$$q_3 = s - m_3^2 = q_1 + q_2,$$

$$p'^2_k = -m_k^2 + \frac{E_k}{E_\gamma} q_k - \frac{q_k^2}{4E_\gamma^2}, \quad k = 1,2,3.$$

The differential rate is then

$$E_\gamma \frac{dR}{d^3 p_\gamma} = \frac{\mathcal{N}}{(2\pi)^7 16 E_\gamma^2} \int ds \int dt |\mathcal{M}(s,t)|^2 \int dE_1 \int dE_2 \frac{f(E_1) f(E_2)(1 + f(E_3))}{[4p'^2_1 p'^2_2 - (p'^2_3 - p'^2_1 - p'^2_2)^2]^{1/2}}.$$

The integration limits on s and t, in addition to $s > (m_1 + m_2)^2$, are such that $q_1 > 0$ and $q_2 > 0$. The limits on E_1, E_2 are set by

$$E_1 > \frac{q_1}{4E_\gamma} + \frac{E_\gamma m_1^2}{q_1}, \quad E_2 > \frac{q_2}{4E_\gamma} + \frac{E_\gamma m_2^2}{q_2}, \quad E_1 + E_2 > E_\gamma + m_3.$$

[1] G. Agakichiev *et al.*, Phys. Rev. Lett. **75**, 1272 (1995); I. Tserruya, Nucl. Phys. **A590**, 127c (1995); A. Drees, *ibid.* **A610**, 536c (1996).

[2] HELIOS-3 Collaboration, M. Masera, spokesman, Nucl. Phys. **A590**, 93c (1995).

[3] NA50 Collaboration, M. Gonin, spokesman, Nucl. Phys. **A610**, 404c (1996).

[4] R. Albrecht *et al.*, Phys. Rev. Lett. **76**, 3506 (1996); R. Santo *et al.*, Nucl. Phys. **A566**, 61c (1994); T. C. Awes *et al.*, *ibid.* **A590**, 81c (1995).

[5] H. Georgi, Nucl. Phys. **B331**, 311 (1990).

[6] G. Q. Li, C. M. Ko, and G. E. Brown, Phys. Rev. Lett. **75**, 4007 (1995); G. Q. Li, C. M. Ko, and G. E. Brown, Nucl. Phys. **A606**, 568 (1996).

[7] G. Q. Li, C. M. Ko, G. E. Brown, and H. Sorge, Nucl. Phys. **A611**, 539 (1996).

[8] G. E. Brown and M. Rho, Phys. Rev. Lett. **66**, 2720 (1991).

[9] T. Hatsuda, H. Shiomi, and H. Kuwaraba, Prog. Theor. Phys. **95**, 1009 (1996).

[10] M. Harada and A. Shibata, Phys. Rev. D **55**, 6716 (1997).

[11] R. Rapp, G. Chanfray, and J. Wambach, Nucl. Phys. **A617**, 472 (1997); Phys. Rev. Lett. **76**, 368 (1996).

[12] See, for example, S. Gottlieb *et al.*, Phys. Rev. D **55**, 6852 (1997).

[13] J. Kapusta, P. Lichard, and D. Seibert, Phys. Rev. D **44**, 2774 (1991).

[14] L. Xiong, E. V. Shuryak, and G. E. Brown, Phys. Rev. D **46**, 3798 (1992).

[15] C. Song, Phys. Rev. C **47**, 2861 (1993).

[16] J. K. Kim, P. Ko, K. Y. Lee, and S. Rudaz, Phys. Rev. D **53**, 4787 (1996).

[17] G. Q. Li and G. E. Brown, Nucl. Phys. **A632**, 153 (1998).

[18] M. Bando, T. Fujiwara, and K. Yamawaki, Prog. Theor. Phys. **79**, 1140 (1988); M. Bando, T. Kugo, and K. Yamawaki, Phys. Rep. **164**, 217 (1988).

[19] K. Kawarabayahi and M. Suzuki, Phys. Rev. Lett. **16**, 255 (1966); Riazuddin and Fayyazuddin, Phys. Rev. **147**, 1071 (1961).

[20] S. Weinberg, Phys. Rev. Lett. **17**, 616 (1966).

[21] Particle Data Group, R. M. Barnett *et al.*, Phys. Rev. D **54**, 1 (1996).

[22] B. R. Holstein, Comments Nucl. Part. Phys. **19**, 239 (1990), and references therein.

[23] C. Adami and G. E. Brown, Phys. Rev. D **46**, 478 (1992).

[24] G. E. Brown, M. Buballa, Z. B. Li, and J. Wambach, Nucl. Phys. **A593**, 295 (1995).

[25] G. E. Brown, M. Buballa, and M. Rho, Nucl. Phys. **A609**, 519 (1996).

[26] C. M. Hung and E. Shuryak, Phys. Rev. C **56**, 453 (1997).

[27] C. M. Ko and G. Q. Li, J. Phys. G **22**, 1673 (1996).

[28] C. M. Ko, V. Koch, and G. Q. Li, Annu. Rev. Nucl. Part. Sci. **47**, 505 (1997).

[29] H. Sorge, H. Stöcker, and W. Greiner, Ann. Phys. (N.Y.) **192**, 266 (1989).

[30] B. J. Verwest and R. A. Arndt, Phys. Rev. C **25**, 1979 (1982).

[31] Gy. Wolf, W. Cassing, and U. Mosel, Nucl. Phys. **A552**, 549 (1993).

[32] P. Danielewicz and G. F. Bertsch, Nucl. Phys. **A533**, 712 (1991).

[33] D. K. Srivastava and B. Sinha, Phys. Rev. Lett. **73**, 2421 (1994); D. K. Srivastava, B. Sinha, and C. Gale, Phys. Rev. C **53**, R567 (1996).

[34] A. Dumitru, U. Katscher, J. A. Maruhn, H. Stöcker, W. Greiner, and D. H. Rischke, Phys. Rev. C **51**, 2166 (1995).